



OPEN

SUBJECT AREAS:  
ELECTRONIC PROPERTIES  
AND DEVICES  
ELECTROCHEMISTRY  
ORGANIC-INORGANIC  
NANOSTRUCTURES

# Hierarchical Nanocomposites of Polyaniline Nanowire Arrays on Reduced Graphene Oxide Sheets for Supercapacitors

Li Wang<sup>1</sup>, Yinjian Ye<sup>1</sup>, Xingping Lu<sup>1</sup>, Zhubiao Wen<sup>1</sup>, Zhuang Li<sup>2</sup>, Haoqing Hou<sup>1</sup> & Yonghai Song<sup>1</sup>

Received

9 September 2013

Accepted

4 December 2013

Published

20 December 2013

Correspondence and requests for materials should be addressed to L.W. (lwangsy2003@hotmail.com) or Y.S. (yhsong@jxnu.edu.cn)

<sup>1</sup>College of chemistry and chemical Engineering, Jiangxi Normal University, 99 Ziyang Road, Nanchang 330022 (P.R. China),  
<sup>2</sup>State Key Lab of Electroanalytical Chemistry, Changchun Institute of Applied Chemistry, Chinese Academy of Sciences, 5625 Renmin Road, Changchun 130022 (P.R. China).

Here we reported a novel route to synthesize a hierarchical nanocomposite (PANI-frGO) of polyaniline (PANI) nanowire arrays covalently bonded on reduced graphene oxide (rGO). In this strategy, nitrophenyl groups were initially grafted on rGO via C-C bond, and then reduced to aminophenyl to act as anchor sites for the growth of PANI arrays on rGO. The functionalized process was confirmed by atomic force microscopy, scanning electron microscopy, Fourier transform infrared spectroscopy, Raman spectroscopy and thermogravimetric analysis. The electrochemical properties of the PANI-frGO as supercapacitor materials were investigated. The PANI-frGO nanocomposites showed high capacitance of  $590 \text{ F g}^{-1}$  at  $0.1 \text{ A g}^{-1}$ , and had no loss of capacitance after 200 cycles at  $2 \text{ A g}^{-1}$ . The improved electrochemical performance suggests promising application of the PANI-frGO nanocomposites in high-performance supercapacitors.

Supercapacitors, also called electrochemical capacitors, have attracted considerable attentions due to their high-power density and long-cycle life. According to the charge storage mechanism, supercapacitors can be classified into two categories: electric double layer capacitors and pseudocapacitors<sup>1</sup>. The former is usually made of carbon-based materials<sup>2-4</sup>, and the capacitance generates from charge separation at the electrode/electrolyte interface. The latter is mainly made of transitional metal oxide<sup>5,6</sup> or conductive polymer<sup>7,8</sup>, and the capacitance generates from fast faradic reaction. To achieve high capacitance, composite materials of carbon and conductive polymers have been used in supercapacitors<sup>9-11</sup>. Among them, graphene, graphene oxide (GO) or reduced graphene oxide (rGO)-polyaniline (PANI) composites have attracted significant attentions<sup>12-16</sup>.

Graphene, a single layer of  $sp^2$ -hybridized carbon atoms, is a promising material for supercapacitors owing to its high conductivity, great mechanical strength and large specific surface. It can provide a long cycle life during the charge/discharge process. However, due to unavoidable aggregation of graphene nanosheets, the capacitance of graphene or graphene derivatives<sup>17,18</sup> is generally  $100\text{--}200 \text{ F g}^{-1}$ . PANI is a famous conducting polymer for supercapacitor owing to its high conductivity, high flexibility, low cost and multi-redox state. It can offer especially high theoretical pseudocapacitances. But its poor stability during the charge/discharge process limits its real application in supercapacitors. The combination of graphene and PANI could overcome the drawbacks of graphene and PANI, and lead to good performance in supercapacitors<sup>19,20</sup>. For example, Wu et al.<sup>19</sup> reported on a graphene/PANI nanofiber exhibited capacitance of  $210 \text{ F g}^{-1}$  at  $0.3 \text{ A g}^{-1}$  and  $194 \text{ F g}^{-1}$  at  $3 \text{ A g}^{-1}$ . Zhang et al.<sup>20</sup> reported on a GO/PANI composites exhibited capacitance of  $320 \text{ F g}^{-1}$  at  $0.1 \text{ A g}^{-1}$ . It was also reported that, compared with randomly connected PANI nanowires, ordered PANI nanowires could reduce the ionic diffusion path, facilitate ionic motion to inner part, and improve unitization of electrode materials<sup>21,22</sup>. Therefore, many efforts have been paid to synthesize ordered PANI on graphene. For example, Xu et al.<sup>22</sup> prepared PANI arrays on GO sheets based on van der Waals force at  $-10^\circ\text{C}$  with capacitance of  $555 \text{ F g}^{-1}$  at  $0.2 \text{ A g}^{-1}$  and  $227 \text{ F g}^{-1}$  at  $2 \text{ A g}^{-1}$ .

Nevertheless, in previous works, most of the graphene-PANI composite materials were connected by non-covalent bond, such as van der Waals force, electrostatic interaction or  $\pi$ - $\pi$  stacking. Compared to non-covalent connection, the covalent connection between PANI and graphene is expected to enhance the electrical conductivity and stability of the composites<sup>23-25</sup>. Only a few studies have dealt with the linkage of graphene and PANI by



using a covalent bond. Recently, PANI-graphene hybrid materials connected by covalent bonds have been reported by Kumar's group<sup>26</sup>. The strategy involved covalently functionalized acylated GO with amine-protected 4-aminophenol, which subsequently polymerized in the presence of aniline monomer to obtain PANI-graphene hybrid materials. Lai et al. has also synthesized PANI-graphene connected by covalent bond<sup>27</sup>. In this method, The  $-NH_2$  groups were introduced to rGO via reacted with ammonia water at  $180^\circ C$ , then an in situ polymerization was used to prepare Amine-modified rGO/PANI. However, a facile method to prepare nanocomposites of vertical PANI array chemically bonded on rGO is still necessary.

Herein, we proposed an effective route to prepare vertical PANI nanowire arrays modified rGO nanocomposites based on covalent connection. First, the rGO was functionalized by spontaneously grafting nitrophenyl groups on rGO based on C-C bond. Then the nitrophenyl groups were reduced to aminophenyl groups, and subsequently polymerization was carried out in the presence of aniline monomer to yield vertical PANI arrays on rGO. A large-scale  $\pi$ - $\pi$  conjugated system is formed between PANI and rGO, which could improve charge transfer significantly. The electrochemical performance of PANI-frGO arrays in supercapacitor was explored in this work.

## Results

Fig. 1A showed the atomic force microscopy (AFM) images of nitrophenyl-rGO nanocomposites. Section analysis revealed that the thickness of nitrophenyl-rGO nanocomposites sheets was about 1.2 nm. Since the length of the nitrophenyl was about  $0.5\text{ nm}^{28}$  and the theoretical thickness of rGO was about  $0.5\text{ nm}^{29}$ , it was reasonable to assume that the nitrophenyl-rGO nanocomposites were consisted of one layer of rGO and monolayer of nitrophenyl groups grafted on both sides of rGO. When nitrophenyl groups were grafted onto the rGO surface parallel to the surface normal axis, the thickness of the nanocomposites should be 1.5 nm. However, the height of nitrophenyl-rGO nanocomposites was only 1.2 nm. Thus it suggested that the nitrophenyl groups could not stand fully perpendicular to the substrate<sup>30</sup>. After these nitrophenyl groups were reduced to aminophenyl groups, it could act as anchor sites to direct the polymerization of aniline for the vertical PANI nanowires array forming on the surfaces of rGO sheets. The AFM image of as-prepared PANI-frGO nanocomposites was shown in Fig. 1B. It obviously showed that PANI nanowires with several ten nanometers in length were almost perpendicular to rGO sheets. Moreover, the vertical PANI arrays were firmly connected to the surface of rGO and did not fall off by exerting large force by AFM tip for many scans<sup>31</sup>.

Fourier transform infrared spectroscopy (FT-IR) was used to confirm the functional groups and PANI on the rGO. As shown in Fig. 2A, the spectrum of GO showed strong absorption at 1729, 1400 and  $1060\text{ cm}^{-1}$  due to C=O vibration in COOH and C-O vibration in COH/COC<sup>32</sup>. A sharp band around  $1625\text{ cm}^{-1}$  might be ascribed to the vibration of residual water. In the spectrum of rGO, the absorption band resulted from oxygen-containing groups disappeared, and new bands at 1577 and  $1215\text{ cm}^{-1}$  attributed to absorbance of C=C and C-C appeared<sup>33</sup>. Compared to the spectrum rGO, the spectrum of nitrophenyl-rGO exhibited new bands at 1517 and  $1342\text{ cm}^{-1}$  which resulted from the symmetric and asymmetric stretching modes of the  $-NO_2$  group, suggesting that nitrophenyl groups were successfully grafted on rGO<sup>34</sup>. For aminophenyl-rGO, it showed new bands at 1630 and  $1302\text{ cm}^{-1}$  attributed to the vibration of N-H and C-N, and a new peak at  $1408\text{ cm}^{-1}$  ascribed to C=C stretching vibration in benzening ring. The result suggested that nitrophenyl groups were successfully reduced to aminophenyl groups. The spectrum of PANI-frGO was shown in Fig. 2B. Two peaks at 1611 and  $1300\text{ cm}^{-1}$  were attributed to the vibrations of C=N and C-N, respectively<sup>26</sup>. The peaks at 800–1100  $\text{cm}^{-1}$  were attributed to the stretching of C-H. The absorbance of C=C stretching deformations of the quinonoid and benzenoid ring vibrations at about 1561 and  $1466\text{ cm}^{-1}$  clearly indicated the presence of PANI on the rGO. The characteristic band attributed to the N-Q-N-Q stretch of the quinonoid ring was also found at  $1170\text{ cm}^{-1}$ . The above results clearly elucidated that the PANI had been covalently grafted onto the surface of rGO sheets<sup>26</sup>. However, it was worth pointing out that the absorbance of C=N, C-N and C=C stretching deformations of the quinonoid and benzenoid ring in PANI-rGO and PANI-frGO was redshifted as compared to that of PANI-GO. The spectral red-shift phenomena of PANI-rGO and PANI-frGO might result from the  $\pi$ - $\pi$  interaction between the rGO sheets and the PANI backbone.

Raman spectroscopy provided a powerful tool to determine the microstructure of carbon-based materials<sup>35</sup> and was employed to analyze the rGO, aminophenyl-rGO and PANI-frGO here. As shown in Fig. 2C, a broad D band at  $1319\text{ cm}^{-1}$  and G band at  $1582\text{ cm}^{-1}$  were observed in the Raman spectrum of rGO. The D band represented the conversion of a  $sp^2$ -hybridized carbon to a  $sp^3$ -hybridized carbon and the G band was related to the in-plane bond-stretching motion of the pairs of  $C\text{ sp}^2$  atoms (the  $E_{2g}$  phonons)<sup>36,37</sup>. The intensity of D band was higher than that of G band due to the defects and partially disordered structure of the rGO. It was worth noting that the intensity ratio (D/G) of aminophenyl-rGO and PANI-frGO increased in comparison with that of the rGO, suggesting that the sheets had lots of defects and disorder structures. It is well agreed with the reported result for functional graphene<sup>38</sup> and proved that the

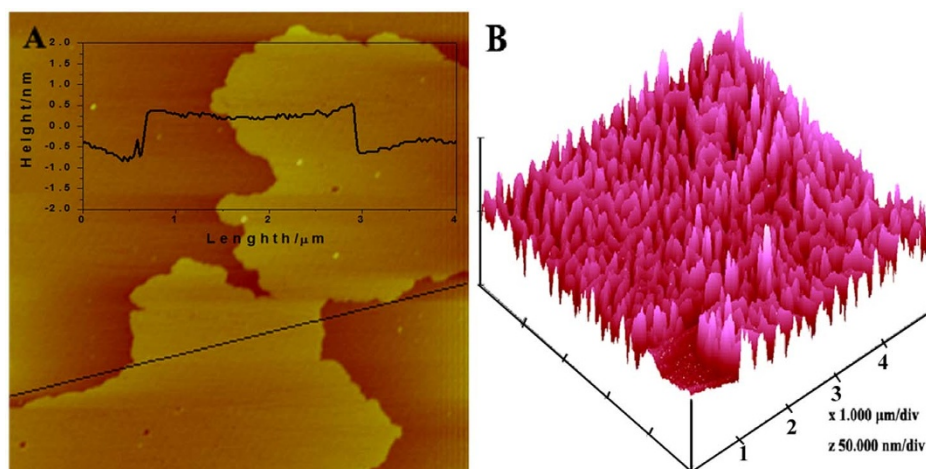


**Figure 1** | AFM images of nitrophenyl-rGO (A) and PANI-frGO (B).

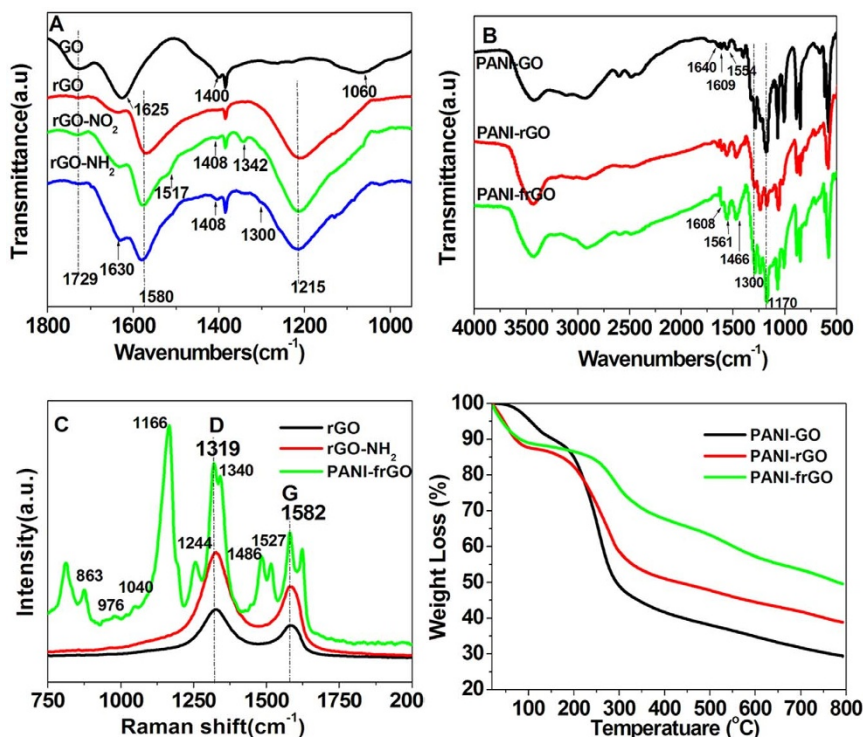


**Figure 2** | (A) FTIR of rGO, nitrophenyl-rGO and aminophenyl-rGO. (B) FTIR of PANI-GO, PANI-rGO and PANI-frGO. (C) Raman of rGO, aminophenyl-rGO and PANI-frGO. (D) TGA curves of PANI-GO, PANI-rGO and PANI-frGO (heating rate = 10 °C/min under a nitrogen atmosphere).

aminophenyl groups and PANI were connected with rGO by chemical bond. Raman scattering was also employed to characterize the presence of PANI in the PANI-frGO. For PANI-frGO, two new peaks at 1527 and 1486 cm<sup>-1</sup> were attributed to C=C stretching and C=N stretching vibration of quinonoid ring, respectively. The stretching band assigned to C-N appeared at 1340 and 1244 cm<sup>-1</sup>. A band at 1040 cm<sup>-1</sup> was attributed to N-H bending in-plane of the benzenoid ring. The peaks at 1166 and 976 cm<sup>-1</sup> were attributed to C-H bending vibration of the benzenoid ring and C-H deformation out-of-plane of the benzenoid ring. The peaks at 890 cm<sup>-1</sup> was assigned to C-N-C wag out-of-plane of the benzenoid ring in EM salt state<sup>31</sup>. All evidences supported that the PANI have been grafted onto the surface of rGO.

The thermal stability of PANI-GO, PANI-rGO and PANI-frGO was investigated by thermogravimetric analysis (TGA). As shown in Fig. 2D, all these materials showed a little mass loss around 100 °C due to the deintercalation of H<sub>2</sub>O. PANI-GO showed a rapid mass loss between 200 and 300 °C due to the decomposition of oxygen-containing groups, such as -OH, -CO-, and -COOH groups. Another reason was ascribed to the partial decomposition of small PANI segments in the nanocomposites. As previous reported<sup>39</sup>, PANI began to decompose at a relatively low temperature less than 150 °C, and was completely oxidized at about 750 °C. The residues of carbonized fragments were remained even at 800 °C. Consequently, a mass loss of 60% between 130 and 750 °C was observed for PANI-GO. Similar TGA features were observed for PANI-rGO, and the mass loss at 200 to 300 °C was ascribed to the oxidative degradation of the nanocomposite itself and the decomposition of the PANI component in the nanocomposites. And the mass loss in this stage was much smaller than that of PANI-GO. The mass loss of PANI-rGO between 130 and 750 °C was 47%. For PANI-frGO nanocomposites, the second stage of mass loss began at 290 °C which was higher than that of PANI-GO and PANI-rGO (about 260 °C). The result demonstrated that the covalent connection resulted in the best thermal stability among these samples. It was worth pointing out that there was hardly any mass loss at 150–250 °C for PANI-frGO, which

demonstrated that the oxygen-containing groups was very rare. It finally displayed a mass loss of 37% between 130 and 750 °C, which was mainly ascribed to the decomposition of the PANI. The above results suggested that the interaction between PANI and rGO based on covalent connection was strongest, and finally played an important role in enhancing the thermal stability of the nanocomposites.

The morphology of the PANI nanowire array on rGO as function of concentration of aniline ( $c_{An}$ ) was investigated. Fig. 3A showed the SEM image of aminophenyl-rGO, and it looks very smooth because the aminophenyl groups were grafted onto rGO to form an ordered monolayer. Fig. 3F showed the SEM image of pure PANI nanofibers, whose diameter was about 80 nm. The PANI nanofibers randomly lied on the substrate to form a network. SEM images of PANI-frGO obtained from different  $c_{An}$  were shown in Fig. 3B–E. At 0.01 M aniline, the sparse and short PANI was generated on rGO surface. As  $c_{An}$  was increased, the PANI nanowire array became longer and longer (Fig. 3C). When the  $c_{An}$  was increased to 0.03 M, the ordered PANI nanowire array with several ten nanometers in length was formed on rGO (Fig. 3D). However, further increasing of  $c_{An}$  (0.04 M) led to a supersaturation state of aniline, which resulted in disordered PANI nanowires on rGO (Fig. 3E). According to the above results, a possible formation mechanism of PANI-frGO nanocomposites was proposed. Herein, there should be two competing nucleation mechanism in PANI-frGO formation: heterogeneous nucleation and homogeneous nucleation. A large number of aminophenyl groups initially grafted on rGO could be used as nucleation sites to anchor PANI on rGO surface. The nucleation sites could minimize the interfacial energy barrier between the solid surface and bulk solution and benefit for polymerization of aniline on a solid surface. Thus, the initial polymerization of aniline tends to adopt heterogeneous nucleation. The ordered monolayer of aminophenyl groups as nucleation sites could play a main role in subsequent polymerization to form vertical PANI array on rGO surface. The vertical PANI array was not observed in previous works in such aniline concentration<sup>38</sup>, suggesting the ordered monolayer of aminophenyl groups directed the oriented polymerization of aniline on the



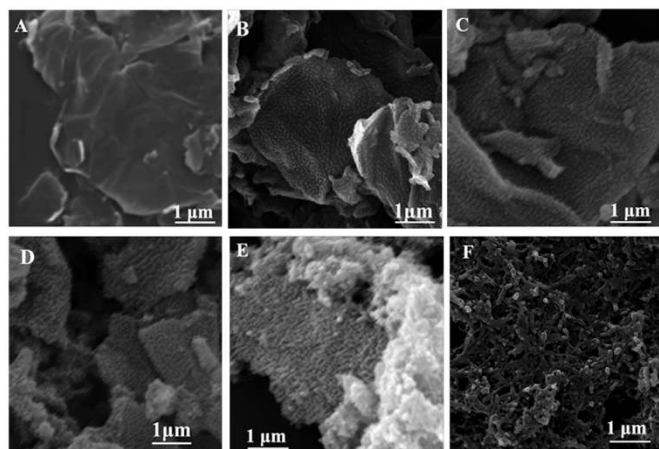


**Figure 3** | SEM images of (A) aminophenyl-rGO and (B–E) PANI-frGO at different concentration of aniline for 3 h: (B) 10 mM, (C) 20 mM, (D) 30 mM and (E) 40 mM, (F) PANI obtained from 40 mM aniline.

rGO<sup>40</sup>. In beginning of polymerization, the aniline monomer in bulk solution polymerized with aminophenyl groups on rGO and formed short PANI. As  $c_{An}$  was increased, the polymerization further occurred to form PANI nanowire array. In case of high concentration of aniline, homogeneous polymerization also took place after the initial nucleation on the solid surface, which resulted in some disordered PANI nanowires on rGO.

To further explore the formation mechanism of the hierarchical nanocomposites, PANI-frGO samples were taken out from the reaction solution at different time intervals during the polymerization process ( $c_{An}$  is 0.03 M). Fig. 4A–E showed the SEM images of PANI-frGO polymerized for 1 h, 1.5 h, 2 h, 3 h and 6 h, respectively. As shown in Fig. 4A, after reaction for 1.0 h, a few short PANI nanowires grew on the surface of rGO. While at 1.5 h, a large amount of PANI nanowires grew uniformly on rGO (Fig. 4B). The PANI nanowires gradually became longer as reaction time increased (Fig. 4C and D). At 3 h, well-ordered PANI nanowires array formed on rGO surface as shown by the high-magnification SEM in Fig. 4F. Further increasing reaction time might lead to the aggregation of individual PANI and form compacted PANI nanowire films on rGO surface (Fig. 4E). The morphology of the PANI-frGO obtained from further increasing reaction time was obviously different from that obtained from further increasing concentration of aniline. Supersaturation state of aniline led to homogeneous polymerization after the initial nucleation on the solid surface and formed disordered PANI nanowires. When suitable concentration of aniline was employed, homogeneous polymerization would not take place even if further increasing reaction time. The formation of compacted PANI nanowire films on rGO surface with further increasing reaction time might be ascribed to the high flexibility of PANI chains. It was very difficult for the longer PANI chains to stand vertically on rGO surface owing to its high flexibility and accordingly a bent structure was more favorable than a straight one as mentioned in previous works<sup>41</sup>. With further increasing reaction time, the vertical PANI nanowires on rGO became longer and longer. The end of PANI chains stacked together to finally form compacted PANI nanowire films on rGO surface.

The potential application of the PANI-frGO nanocomposites as electrode materials for supercapacitors was tested by standard cyclic voltammetry (CV), electrochemical impedance spectroscopy (EIS) and galvanostatic charge/discharge. Fig. 5A showed the CVs of PANI, PANI-GO, PANI-rGO and PANI-frGO electrodes with same weight, respectively. Two pairs of redox waves related to reversible charge–discharge behaviour and pseudocapacitance characteristic of PANI were observed in four electrodes. The pair of peaks  $O_1/R_1$  was

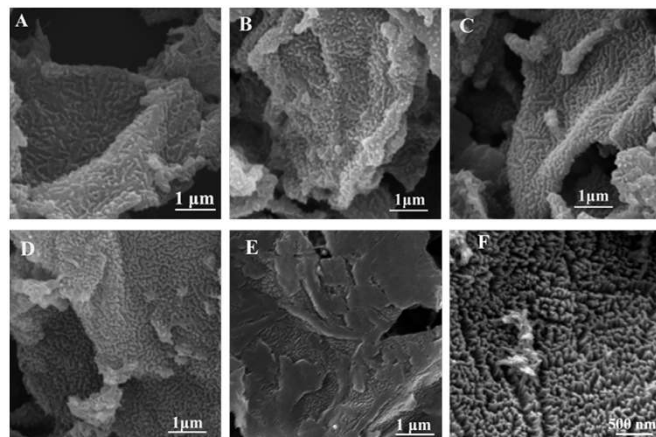


**Figure 4** | SEM images of PANI-frGO obtained at different reaction intervals: 1 h (A), 1.5 h (B), 2 h (C), 3 h (D), 6 h (E), (F) high-magnification SEM image of PANI-frGO obtained at 3 h.

attributed to the redox transition of PANI between leucoemeraldine and emeraldine. Another pair of peaks  $O_2/R_2$  was derived from the emeraldine–pernigraniline transformation. The peak current of PANI-GO electrode, PANI-rGO electrode and PANI-frGO electrode were higher than that of pure PANI electrode, indicating that the rGO and GO could effectively increase the capacitance of PANI. In comparison, the CV of PANI-frGO electrode exhibited a much larger rectangular area than that of PANI-GO electrode and PANI-rGO electrode, mainly due to its chemical bonding and ordered morphology. The large-scale  $\pi$ - $\pi$  conjugation between PANI and rGO facilitated charge transfer and consequently improved electrochemical performance significantly.

The specific capacitance ( $C_{spec}$ ) values were calculated from the charging and discharging curves (Fig. 5B and C) according to the following equation<sup>16</sup>

$$C_s = \frac{I\Delta t}{\Delta V \times m} \quad (1)$$

where  $I$  was the constant discharge current (A),  $\Delta t$  was the discharge time (s),  $\Delta V$  was the potential change during discharge process, and  $m$  was the mass of the active materials within the electrode (g). Fig. 5B showed the galvanostatic charge/discharge curves of PANI, PANI-GO, PANI-rGO and PANI-frGO at 0.1 A g<sup>-1</sup>. Fig. 5C showed charge/discharge curves of frGO-PANI at various current densities. The specific capacitances of PANI, PANI-GO, PANI-rGO and PANI-frGO calculated from their charge/discharge curves were shown in Fig. 5D. At 0.1 A g<sup>-1</sup>, the specific capacitance of PANI-frGO (590 F g<sup>-1</sup>) was much higher than that of PANI-GO (262 F g<sup>-1</sup>) and PANI-rGO (322 F g<sup>-1</sup>). At the same time, the specific capacitance of pure PANI was 215 F g<sup>-1</sup>. At 1 A g<sup>-1</sup>, the specific capacitance of PANI-frGO (360 F g<sup>-1</sup>) was still much higher than that of PANI-GO (220 F g<sup>-1</sup>) and PANI-rGO (259 F g<sup>-1</sup>). The results suggested that chemical bond and array morphology greatly promoted the capacitance of the PANI-frGO hybrid materials.

The cycle life of PANI, PANI-GO, PANI-rGO and PANI-frGO were conducted at 2 A g<sup>-1</sup>. As displayed in Fig. 5E, PANI-frGO showed good cyclability without loss of capacitance over 200 cycles. After 1000 cycles, the specific capacitances of PANI-frGO retained 91%, which was much higher than that of pure PANI (69%), PANI-GO (84%) and PANI-rGO (81%).

EIS was used to further study the internal resistance, charge transfer kinetics, and ion diffusion process of PANI, PANI-GO, PANI-rGO and PANI-frGO electrodes. The EIS was measured in a frequency range of 10 kHz to 10 mHz. As shown in Fig. 5F, the intercept between the impedance spectrum and real impedance axis

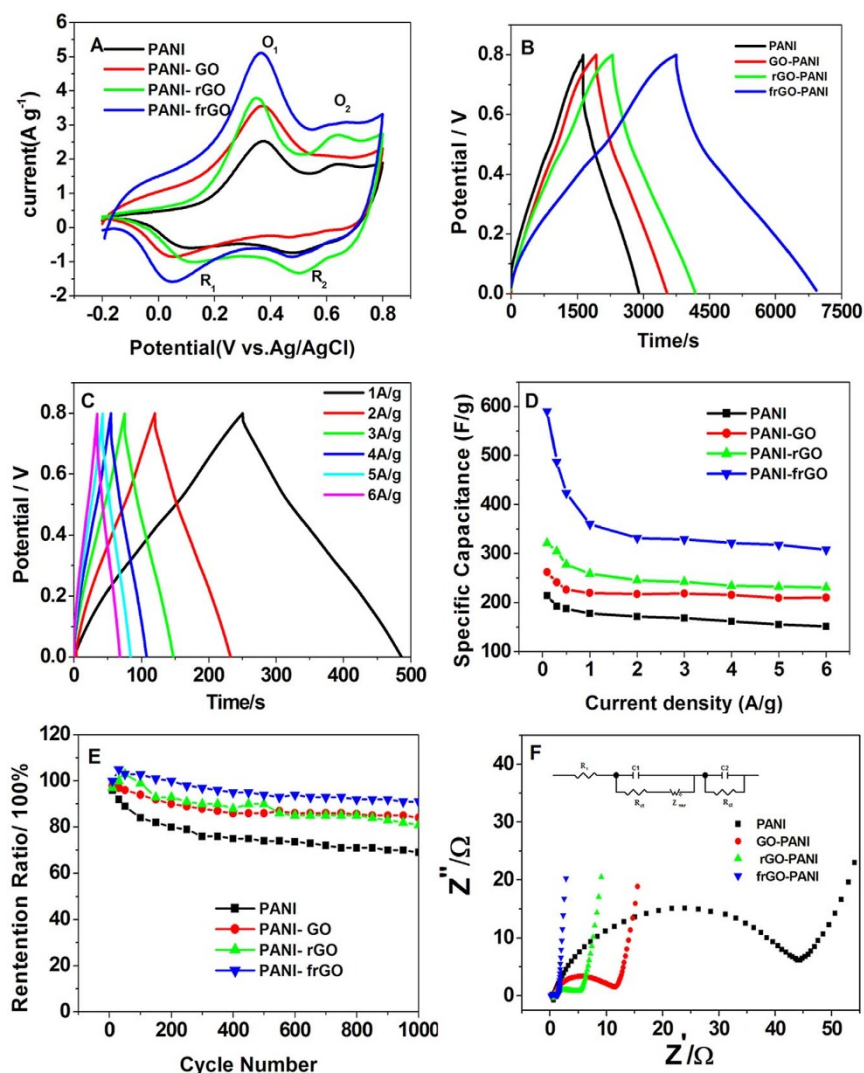


**Figure 5** | Electrochemical capacitance performance of PANI-frGO obtained at  $c_{An} = 30$  mM,  $t_r = 3$  h. (A) CV curves of PANI, PANI-GO, PANI-rGO and PANI-frGO at a scan rate of  $5$  mV  $s^{-1}$ . (B) Charge-discharging curves of PANI, PANI-GO, PANI-rGO and PANI-frGO at  $0.1$  A  $g^{-1}$ . (C) Charge-discharging curves of PANI-frGO at different current densities. (D) Specific capacitance plots at different current densities. (E) Plots of cycle life test of PANI, PANI-GO, PANI-rGO and PANI-frGO. (F) Nyquist plots of supercapacitors based on PANI, PANI-GO, PANI-rGO and PANI-frGO.

( $Z'$ ) was very small (about  $0.6$  Ohm) for all the four electrodes. The small intercept indicated that the series resistance, which included the electrolyte solution resistance and contact resistance at the interface of active material/current collector, was very low for all four electrodes. All of the Nyquist plots of the four nanocomposite electrodes showed an incomplete semicircle in the high-frequency region and straight line in the low-frequency region. The semicircle impedance plots were associated with charge transfer resistance at the electrode/solution interface, while the straight line was determined by ion diffusion. Among the four nanocomposite electrodes, the slope of the straight line for PANI-frGO electrode was largest, closest to the imaginary impedance axis ( $Z''$ ). The diameter of semicircle for PANI-frGO electrode was smallest. The results implied that PANI-frGO exhibited the highest conductivity or lowest internal resistance, including polarization impedance.

The Nyquist plots of all the four electrodes could be well-modeled using a complex equivalent circuit, as shown by the inset in Fig. 5F.  $R_s$  was the series solution resistance, which included the electrolyte resistance and the active material/current collector contact resistance.  $C_1$  represented double-layer capacitance and  $C_2$  represented Faradic capacitance.  $R_{ct}$  in parallel to  $C$  was the charge transfer

resistance at the electrode/solution interface. These components formed a mixed-controlled Randles circuit, which was usually used to model capacitance in a process with a combination of kinetic and diffusion processes determining the rate. At high frequencies, the capacitor impedance became much smaller and the system resistance was dominated by the resistors and polarization impedances. At low frequencies, an ideal polarizable capacitance would give a straight line with large angles with respect to  $Z'$  or almost parallel to  $Z''$ . It was noted that in Fig. 5F the semicircles partially (in the mid-frequency region) disappeared. The absence of the semicircle in the complex impedance plane had been reported and was explained by high ionic conductivity at the electrode/electrolyte interface<sup>42</sup>. In the PANI-frGO case, the  $R_s$  and  $R_{ct}$  was the lowest among the four composites. And the phase angle increased continuously as further decreased in frequency. This meant that the contribution of polarization impedance reduced (the kinetic and charge transfer were no longer rate-determining steps), while mass capacitance remained the dominant component of the system impedance. The largest slope of vertical curve for PANI-frGO indicated that PANI-frGO could provide the best capacitance. As discussed above, we might conclude that PANI-frGO was the best electrode material for supercapacitor appli-



Table 1 | Comparison of the capacitances based on graphene-PANI

Materials	morphologies	Connecting mode	Specific capacitance (F g <sup>-1</sup> )	Cycle life	Ref
rGO/PANI <sup>a</sup>	nanoparticles	Non-covalently	361 at 0.3 A g <sup>-1</sup>	82% after 1000 cycles at 0.3 A g <sup>-1</sup>	[44]
GO-PANI <sup>b</sup>	nanoparticles	Non-covalently	425 at 0.2 A g <sup>-1</sup>	83% after 500 cycles at 1 A g <sup>-1</sup>	[45]
Graphene/Polyaniline <sup>c</sup>	nanoparticles	Non-covalently	257 at 0.1 A g <sup>-1</sup>	98% after 1000 cycles at 2 A g <sup>-1</sup>	[46]
Porous Graphene/Polyaniline <sup>d</sup>	nanowires	Non-covalently	385 at 0.5 A g <sup>-1</sup>	—	[47]
sGNS/cMWCNT/PANI <sup>e</sup>	nanotubes	Non-covalently	107 at 1 A g <sup>-1</sup>	91% after 5000 cycles	[48]
PANI-GO-CNT <sup>f</sup>	nanosheets	Non-covalently	589 at 0.2 A g <sup>-1</sup>	81% after 1000 cycles	[49]
Graphene oxide doped PANI <sup>g</sup>	nanofibers	Non-covalently	531 at 0.2 A g <sup>-1</sup>	—	[13]
PANI/rGO <sup>h</sup>	nanorod	Non-covalently	970 at 2.5 A g <sup>-1</sup>	90% after 1700 cycles at 1 A g <sup>-1</sup>	[16]
PANI arrays on GO <sup>i</sup>	nanowires	Non-covalently	555 at 0.2 A g <sup>-1</sup>	92% after 2000 cycles at 1 A g <sup>-1</sup>	[22]
Amide group-connected graphene-PANI <sup>j</sup>	nanofibers	Covalently	579.8 at 0.3 A g <sup>-1</sup>	96% after 200 cycles at 3 A g <sup>-1</sup>	[25]
PANI grafted rGO <sup>k</sup>	rod-like	Covalently	250 at 100 mV s <sup>-1</sup>	—	[26]
Amine-modified rGO/PANI <sup>l</sup>	nanofibers	Covalently	388 at 1 A g <sup>-1</sup>	no lose over 680 cycles at 2 mV s <sup>-1</sup>	[27]
PANI-grafted graphene with amide groups <sup>m</sup>	nanowires	Covalently	623.1 at 0.1 A g <sup>-1</sup>	no lose over 500 cycles at 50 A g <sup>-1</sup>	[31]
PANI-rGO	nanowires	Covalently	590 at 0.1 A g <sup>-1</sup>	91% after 1000 cycles at 2 A g <sup>-1</sup>	This work

<sup>a</sup>PANI were directly coated on rGO via in situ polymerization process.

<sup>b</sup>The nanocomposite were prepared by in situ polymerization with the assistance of supercritical carbon dioxide (SC CO<sub>2</sub>).

<sup>c</sup>Graphene/polyaniline (PANI) nanocomposites were prepared by reducing graphene oxide with hydrazine in the presence of different amounts of polyaniline nanoparticles.

<sup>d</sup>CaCO<sub>3</sub> particles formed in situ in GO dispersion to obtain porous Graphene. Then Porous Graphene/Polyaniline was synthesized via in situ polymerization.

<sup>e</sup>sGNS/cMWCNT/PANI synthesized via in situ polymerization.

<sup>f</sup>PANI-GO-CNT was synthesized by a one-step process using a simplified template-free polymerization method.

<sup>g</sup>PANI doped with GO sheets was synthesized via in situ polymerization of monomer in the presence of GO [mass ratio of aniline/GO is 100 : 1].

<sup>h</sup>The microelectrodes of the supercapacitor are prepared by in situ electrodeposition of polyaniline (PANI) nanorods on the surface of rGO patterns that are fabricated by micromolding in capillaries.

<sup>i</sup>PANI arrays on GO was synthesized via in situ polymerization at -10 °C.

<sup>j</sup>Graphene is activated using SOCl<sub>2</sub> and reacts with PANI to form an amide group that intimately connects graphene and PANI.

<sup>k</sup>GO was acylated in the presence of excess SOCl<sub>2</sub> and then reacted with amine-protected 4-aminophenol, following the deprotection of amine groups, an in situ polymerization was carried out to obtain PANI-rGO.

<sup>l</sup>The -NH<sub>2</sub> groups were introduced to rGO via reacted with ammonia water at 180 °C, then an in situ polymerization was used to prepare Amine-modified rGO/PANI.

<sup>m</sup>The GO is activated using SOCl<sub>2</sub> and reacts with PANI to form PANI-GO, then reduced to PANI-rGO.



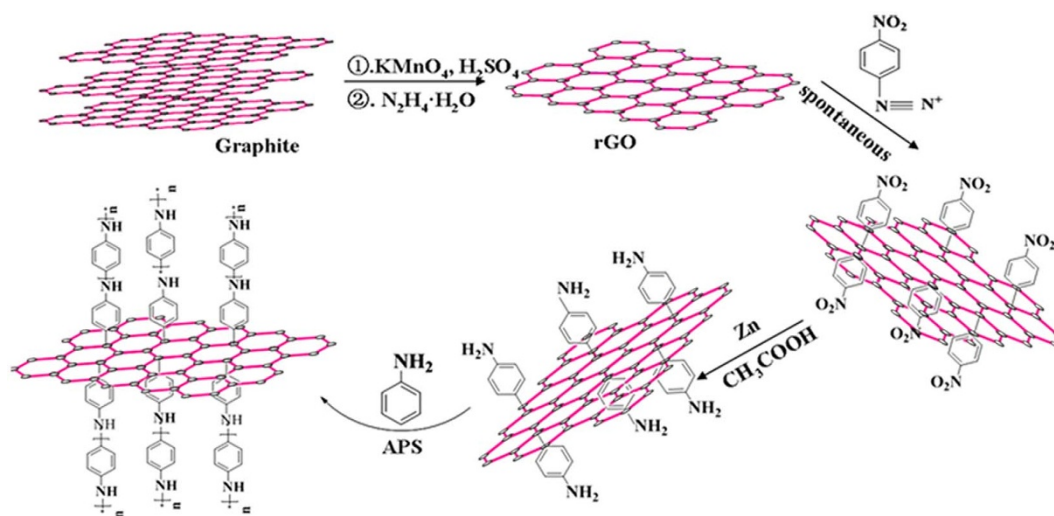


**Figure 6** | Procedure for the fabrication of PANI-frGO.

cations, owing to low internal resistance, very good charge transfer and excellent ionic conductivity.

## Discussion

To date, many supercapacitors based on graphene-PANI nanocomposites have been developed and all of them have advantages and limitations. The performances of the capacitances based on graphene-PANI nanocomposites were listed in Table 1. Obviously, the properties of the capacitances strongly depend on the morphology of PANI on the graphene surface, the connecting mode between PANI and graphene, and the mass ratio of PANI and graphene. As shown in Table 1, various morphologies such as nanoparticles<sup>44–46</sup>, nanowires<sup>47</sup>, nanofibers<sup>13,22</sup>, nanotubes<sup>48</sup>, nanosheets<sup>49</sup> exhibited obvious different results. It indicated that the morphology had a great impact on the capacitance of the graphene-PANI because the ionic diffusion path was different in various morphologies. Moreover, the connecting mode (non-covalent connecting and covalent connecting) might be critical to the capacitance of the graphene-PANI. Compared to covalent connecting, non-covalent connecting was weaker and lacked a  $\pi$ - $\pi$  conjugated system between PANI and rGO. It might have a negative impact on the capacitance and cycle life of the material. In addition, the mass ratio of PANI and graphene also affected the capacitance of the graphene-PANI greatly, since the capacitance of the nanocomposites might mainly derive from the pseudocapacitance of PANI. Generally speaking, the capacitance of the graphene-PANI was affected by various parameters together. In our strategy, the covalent connecting between PANI and rGO and the vertical PANI nanowire array improved the capacitance and cycle life more than other graphene-PANI nanocomposites together. It suggested that our product has certain advantages among the materials from various synthesis routes.

Except for application in supercapacitors, the PANI-frGO obtained from our strategy might also have many potential applications due to the enhanced properties of rGO and PANI. Recently many graphene-based hybrid materials with superior properties such as Au cluster/graphene<sup>50</sup>, metal oxide nanoparticle/graphene<sup>51</sup> and Co-porphyrin multilayers/rGO<sup>52</sup> have been investigated and used in oxygen reduction reaction and capacitive deionization. Therefore, the PANI-frGO containing unique properties of rGO and PANI could also act as specific supports to form hybrid nanocomposites. The PANI-frGO-based materials were also expected for use in sensors, solar cells, lithium ion batteries, fuel cells.

In summary, we have developed a novel method to obtain PANI-frGO hybrid materials based on a chemical bond. AFM and SEM revealed that the vertical PANI nanowire array was grafted on rGO

sheets. TGA results showed that the PANI-frGO nanocomposites were more thermally stable than the two nanocomposites connected by van der Waals force. The results of the galvanostatic charge/discharge tests illustrated the higher specific capacitances and longer cycle life of the PANI-frGO hybrid materials than the two nanocomposites connected by van der Waals force. With enhanced performance, this hierarchical nanocomposite might have great potential applications.

## Methods

**Materials.** Graphite powder (spectrum pure) was purchased from Sinopharm Chemical Reagent Company (Shanghai, China). Nitrophenyl diazonium tetrafluoroborate and tetrabutylammonium were obtained from Sigma-Aldrich (St. Louis, USA). Aniline, ammonium peroxydisulfate, Zn powder (>90%), H<sub>2</sub>SO<sub>4</sub> (98%), CH<sub>3</sub>COOH (>99.5%) and CH<sub>3</sub>CH<sub>2</sub>OH (>99.7%) were purchased from Shanghai Chemical Reagent Company (Shanghai, China). Aniline was distilled under reduced pressure and other reagents were used as received without further treatment. All aqueous solutions were prepared with ultra-pure water, purified by a Millipore-Q system (18.2 M $\Omega$  cm<sup>-1</sup>).

**Instrumentation.** Atomic force microscopy (AFM) measurements were carried out with an AJ-III (Shanghai Aijian Nanotechnology, China) using a tapping mode. Standard silicon cantilevers (spring constant 0.6–6 N m<sup>-1</sup>) were used under their resonance frequency (typically, 60–150 kHz). All AFM images were acquired under ambient conditions, and images were raw data except for flattening. The scanning electron microscopy (SEM) analysis was taken using a XL30 ESEM-FEG SEM at an accelerating voltage of 20 kV equipped with a Phoenix energy dispersive x-ray analyzer (EDXA). FTIR spectroscopy was recorded on a Perkin-Elmer Spectromer 100 spectrometer (Perkin-Elmer Company, USA) using KBr pellets. Raman spectra were performed at room temperature with a MicroRaman System RM3000 spectrometer and an argon ion laser operating at a wavelength of 514 nm as the excitation. The decomposition patterns were determined thermogravimetrically using a TGA analyzer (Q200, TA Instruments, USA) at a ramp rate of 10 °C min<sup>-1</sup> in nitrogen. All electrochemical tests were carried out on a CHI 660 C electrochemical workstation (Shanghai, China) in 2 M H<sub>2</sub>SO<sub>4</sub> aqueous solution with three-electrode cells where Pt wire serves as the counter electrode and Ag/AgCl as the reference electrode. The working electrodes were prepared by mixing products with acetylene black and polytetrafluoroethylene (PTFE) (mass ratio of 85:10:5). The mixture was kneaded to obtain a paste, and then the paste was pressed onto the SS sheet (1 cm<sup>2</sup>) at 10 MPa for 1 min in order to assure a good electrical contact. The mass of active ranges from 2 mg to 6 mg. EIS was characterized at open circuit potential in the frequency range from 10<sup>5</sup> Hz to 0.01 Hz.

**Synthesis of GO and rGO.** GO was synthesized according to previous methods<sup>45</sup>. Briefly, graphite powder (1.0 g) was dispersed into 23 mL concentrated H<sub>2</sub>SO<sub>4</sub> (18.0 M) in an ice bath. Then, KMnO<sub>4</sub> (3.0 g) was gradually added into the above solution under continuous vigorous stirring at a temperature below 20 °C. After that, the ice bath was replaced by an oil bath and the mixture was heated to 35 °C for 30 min under continuous stirring. Then, ultra-pure water was slowly added into the above solution, which produced a rapid increase in solution temperature up to a maximum of 100 °C. The reaction was maintained at 98 °C for a further 15 min, and terminated by the sequential addition of more ultra-pure water (140 mL in total) and H<sub>2</sub>O<sub>2</sub> (30%, 10 mL). The solid product was separated by centrifugation at 5000 rpm and washed



with 5% HCl until  $\text{SO}_4^{2-}$  ions were no longer detectable with  $\text{BaCl}_2$ . Finally, the solid product was washed three times with acetone and dried overnight at  $65^\circ\text{C}$ . The rGO was prepared by reduction of GO with hydrazine. Typically, hydrazine (0.12 mL) was added into the dispersion of GO (100 mg GO in 100 mL water) and sonicated for 1 h. Then the mixture was reacted at  $90^\circ\text{C}$  under constant stirring for 1 h. rGO was obtained by filtering the product and drying in vacuum. The procedure was shown in Fig. 6.

**Synthesis of nitrophenyl-rGO nanocomposites.** The nitrophenyl-rGO nanocomposites were prepared by spontaneous grafting nitrophenyl groups to the basal carbon atoms according to previous procedure<sup>34</sup>. Briefly, rGO (12 mg) was dispersed in 10 mL degassed acetonitrile by ultrasonication for about 1 h. Then nitrophenyl diazonium tetrafluoroborate (24 mg) and tetrabutylammonium (0.329 mg) were added into above solution. The mixtures were placed in a glove box in the absence of light for 5 h. The nitrophenyl-rGO was obtained by filtering the product and washing with acetonitrile and acetone and drying at  $80^\circ\text{C}$  for 4 h. The procedure was shown in Fig. 6.

**Synthesis of aminophenyl-rGO nanocomposites.** The aminophenyl-rGO was prepared by reduction of nitrophenyl-rGO with Zn in  $\text{CH}_3\text{COOH}$  solution. Briefly, The nitrophenyl-rGO (6 mg) was dispersed in 20 mL  $\text{CH}_3\text{COOH}-\text{H}_2\text{O}$  (3:2) by ultrasonication, then Zn (104 mg),  $\text{NH}_4\text{Cl}$  (1 mg) and  $\text{CH}_3\text{COOH}$  (2.3 mL) were added. The mixture solution was refluxed at  $60^\circ\text{C}$  for 3 h. The product was centrifuged and washed with 0.1 M HCl and ultra-pure water three times each and dried at  $60^\circ\text{C}$  for 4 h in an oven. The procedure was shown in Fig. 6.

**Synthesis of PANI-frGO.** PANI-frGO composite were produced by in situ polymerization of aniline. The aminophenyl-rGO (3.4 mg) were dispersed in a 5 mL aqueous solution containing aniline and  $\text{H}_2\text{SO}_4$  (1 M). Then another 5 mL aqueous solution containing ammonium persulfate (APS) was added in, and stirred for a while. The molar ratio of aniline/APS was 4/1. The polymerization was carried out under nitrogen in an ice-water bath with the temperature  $0-5^\circ\text{C}$ . After polymerization for about 3 h, the composite cloths were collected, washed with water and ethanol and dried at  $60^\circ\text{C}$  for 6 h. A series of PANI-frGO were prepared in a solution with different aniline concentrations (The  $c_{\text{An}}$  was 0.01 M, 0.02 M, 0.03 M and 0.04 M, respectively). The similar method was used to obtain PANI-GO and PANI-rGO. The procedure was shown in Fig. 6.

- Conway, B. E. Transition from “supercapacitor” to “battery” behavior in electrochemical energy storage. *J. Electrochem. Soc.* **138**, 1539–1548 (1991).
- Frackowiak, E. Carbon materials for supercapacitor application. *Phys. Chem. Chem. Phys.* **9**, 1774–1785 (2007).
- Weng, Z. *et al.* Graphene-cellulose paper flexible supercapacitors. *Adv. Energy Mater.* **1**, 917–922 (2011).
- Hahm, M. G. *et al.* Carbon nanotube – nanocup hybrid structures for high power supercapacitor applications. *Nano Lett.* **12**, 5616–5621 (2012).
- Yan, J. *et al.* Fast and reversible surface redox reaction of graphene– $\text{MnO}_2$  composites as supercapacitor electrodes. *Carbon* **48**, 3825–3833 (2010).
- Zhang, X. *et al.* High performance asymmetric supercapacitor based on  $\text{MnO}_2$  electrode in ionic liquid electrolyte. *J. Mater. Chem. A* **1**, 3706–3712 (2013).
- Nyholm, L., Nystrom, G., Mihiranyan, A. & Stromme, M. Toward flexible polymer and paper-based energy storage devices. *Adv. Mater.* **23**, 3751–3769 (2011).
- Roberts, M. E., Wheeler, D. R., McKenzie, B. B. & Bunker, B. C. High specific capacitance conducting polymer supercapacitor electrodes based on poly(tris(thiophenylphenyl)amine). *J. Mater. Chem.* **19**, 6977–6979 (2009).
- Wang, G., Zhang, L. & Zhang, J. A review of electrode materials for electrochemical supercapacitors. *Chem. Soc. Rev.* **41**, 797–828 (2012).
- Kuilla, T. *et al.* Recent advances in graphene based polymer composites. *Prog. Polym. Sci.* **35**, 1350–1375 (2010).
- Huang, F. & Chen, D. Towards the upper bound of electrochemical performance of ACNT@polyaniline arrays as supercapacitors. *Energ. Environ. Sci.* **5**, 5833–5841 (2012).
- Wang, D. W. *et al.* Fabrication of graphene/polyaniline composite paper via in situ anodic electropolymerization for high-performance flexible electrode. *ACS Nano* **3**, 1745–1752 (2009).
- Wang, H., Hao, Q., Yang, X., Lu, L. & Wang, X. Graphene oxide doped polyaniline for supercapacitors. *Electrochem. Commun.* **11**, 1158–1161 (2009).
- Feng, X.-M. *et al.* One-step electrochemical synthesis of graphene/polyaniline composite film and its applications. *Adv. Funct. Mater.* **21**, 2989–2996 (2011).
- Sarker, A. K. & Hong, J. D. Layer-by-layer self-assembled multilayer films composed of graphene/polyaniline bilayers: high-energy electrode materials for supercapacitors. *Langmuir* **28**, 12637–12646 (2012).
- Xue, M. *et al.* Structure-based enhanced capacitance: in situ growth of highly ordered polyaniline nanorods on reduced graphene oxide patterns. *Adv. Funct. Mater.* **22**, 1284–1290 (2012).
- Wang, Y. *et al.* Supercapacitor devices based on graphene materials. *J. Phys. Chem. C* **113**, 13103–13107 (2009).
- Stoller, M. D., Park, S., Zhu, Y., An, J. & Ruoff, R. S. Graphene-based ultracapacitors. *Nano Lett.* **8**, 3498–3502 (2008).
- Wu, Q., Xu, Y. X., Yao, Z. Y., Liu, A. R. & Shi, G. Q. Supercapacitors based on flexible graphene/polyaniline nanofiber composite films. *ACS Nano* **4**, 1963–1970 (2010).
- Zhang, K., Zhang, L. L., Zhao, X. S. & Wu, J. Graphene/polyaniline nanofiber composites as supercapacitor electrodes. *Chem. Mater.* **22**, 1392–1401 (2010).
- Zhang, H., Cao, G., Wang, Z., Yang, Y., Shi, Z. & Gu, Z. Tube-covering-tube nanostructured polyaniline/carbon nanotube array composite electrode with high capacitance and superior rate performance as well as good cycling stability. *Electrochem. Commun.* **10**, 1056–1059 (2008).
- Xu, J. J., Wang, K., Zu, S. Z., Han, B. H. & Wei, Z. X. Hierarchical nanocomposites of polyaniline nanowire arrays on graphene oxide sheets with synergistic effect for energy storage. *ACS Nano* **4**, 5019–5026 (2010).
- Shreyam, C., Rama, K. L. & Arun, K. N. Changing the morphology of polyaniline from a nanotube to a flat rectangular nanorip by polymerizing in the presence of amino-functionalized reduced graphene oxide and its resulting increase in photocurrent. *Carbon* **52**, 509–519 (2013).
- Lai, L. F. *et al.* One-step synthesis of  $\text{NH}_2$ -graphene from in situ graphene-oxide reduction and its improved electrochemical properties. *Carbon* **49**, 3250–3257 (2011).
- Jianhua, L. *et al.* Preparation of an amide group-connected graphene-polyaniline nanofiber hybrid and its application in supercapacitors. *ACS Appl. Mater. Inter.* **4**, 2870–2876 (2012).
- Kumar, N. A. *et al.* Polyaniline-grafted reduced graphene oxide for efficient electrochemical supercapacitors. *ACS Nano* **6**, 1715–1723 (2012).
- Lai, L. F. *et al.* Preparation of supercapacitor electrodes through selection of graphene surface functionalities. *ACS Nano* **6**, 5941–5951 (2012).
- Chen, X., Liu, S., Song, Y. & Dong, S. Fabrication and characterization of ordered oligoaniline film. *Chem. Lett.* **31**, 552–553 (2002).
- Geim, A. K. & Novoselov, K. S. The rise of graphene. *Nature Mater.* **6**, 183–191 (2007).
- Song, Y., Liu, Y., Yang, M., Zhang, B. & Li, Z. Diluting thiol-derivatized oligonucleotide monolayers on Au(111) by mercaptohexanol replacement reaction. *Appl. Surf. Sci.* **252**, 5693–5699 (2006).
- An, J. *et al.* Polyaniline-grafted graphene hybrid with amide groups and its use in supercapacitors. *J. Phys. Chem. C* **116**, 19699–19708 (2012).
- Titelman, G. I. *et al.* Characteristics and microstructure of aqueous colloidal dispersions of graphite oxide. *Carbon* **43**, 641–649 (2005).
- Guo, Y. J. *et al.* Cyclodextrin functionalized graphene nanosheets with high supramolecular recognition capability: Synthesis and host-guest inclusion for enhanced electrochemical performance. *ACS Nano* **4**, 4001–4010 (2010).
- Bekyarova, E. *et al.* Chemical modification of epitaxial graphene: spontaneous grafting of aryl groups. *J. Am. Chem. Soc.* **131**, 1336–1337 (2009).
- Yan, X., Chen, J., Yang, J., Xue, Q. & Miele, P. Fabrication of free-standing, electrochemically active, and biocompatible graphene oxide-polyaniline and graphene-polyaniline hybrid papers. *ACS Appl. Mater. Inter.* **2**, 2521–2529 (2010).
- Ferrari, A. & Robertson, J. Interpretation of Raman spectra of disordered and amorphous carbon. *Phys. Rev. B* **61**, 14095–14107 (2000).
- Cancado, L., Pimenta, M., Neves, B., Dantas, M. & Jorio, A. Influence of the atomic structure on the Raman spectra of graphite edges. *Phys. Rev. Lett.* **93**, 247401–247405 (2004).
- Yan, J. *et al.* Preparation of a graphene nanosheet/polyaniline composite with high specific capacitance. *Carbon* **48**, 487–493 (2010).
- Gheno, G., de Souza Basso, N. R. & Hübner, R. Polyaniline/graphite nanocomposites: synthesis and characterization. *Macromol. Symp.* **299–300**, 74–80 (2011).
- Chiou, N.-R., Lu, C., Guan, J., Lee, L. J. & Epstein, A. J. Growth and alignment of polyaniline nanofibers with superhydrophobic, superhydrophilic and other properties. *Nat. Nanotechnol.* **2**, 354–357 (2007).
- Lee, J. I. *et al.* Highly Aligned Ultrahigh Density Arrays of Conducting Polymer Nanorods using Block Copolymer Templates. *Nano Lett.* **8**, 2316–2320 (2008).
- Li, X., Rong, J. & Wei, B. Electrochemical behavior of single-walled carbon nanotube supercapacitors under compressive stress. *ACS Nano* **4**, 6039–6049 (2010).
- Hummers Jr, W. S. & Offeman, R. E. Preparation of graphitic oxide. *J. Am. Chem. Soc.* **80**, 1339–1339 (1958).
- Zhang, J. & Zhao, X. S. Conducting polymers directly coated on reduced graphene oxide sheets as high-performance supercapacitor electrodes. *J. Phys. Chem. C* **116**, 5420–5426 (2012).
- Xu, G. H. *et al.* Preparation of Graphene Oxide/Polyaniline Nanocomposite with Assistance of Supercritical Carbon Dioxide for Supercapacitor Electrodes. *Ind. Eng. Chem. Res.* **51**, 14390–14398 (2012).
- Li, Z. F., Zhang, H., Liu, Q., Sun, L., Stanciu, L. & Xie, J. Fabrication of high-surface-area graphene/polyaniline nanocomposites and their application in supercapacitors. *ACS Appl. Mater. Interf.* **5**, 2685–91 (2013).
- Meng, Y., Wang, K., Zhang, Y. & Wei, Z. Hierarchical Porous Graphene/Polyaniline Composite Film with Superior Rate Performance for Flexible Supercapacitors. *Adv. Mater.* DOI: 10.1002/adma.201303529 (2013).
- Shen, J., Yang, C., Li, X. & Wang, G. High-performance asymmetric supercapacitor based on nanoarchitected polyaniline/graphene/carbon nanotube and activated graphene electrodes. *ACS Appl. Mater. Interf.* **5**, 8467–76 (2013).





49. Ning, G., Li, T., Yan, J., Xu, C., Wei, T. & Fan, Z. Three-dimensional hybrid materials of fish scale-like polyaniline nanosheet arrays on graphene oxide and carbon nanotube for high-performance ultracapacitors. *Carbon* **54**, 241–248 (2013).
50. Yin, H. J., Tang, H. J., Wang, D., Gao, Y. & Tang, Z. Y. Facile Synthesis of Surfactant-Free Au Cluster/Graphene Hybrids for High-Performance Oxygen Reduction Reaction. *ACS Nano* **6**, 8288–8297 (2013).
51. Yin, H. J. *et al.* Three-Dimensional Graphene/Metal Oxide Nanoparticle Hybrids for High-Performance Capacitive Deionization of Saline Water. *Adv. Mater.* DOI: 10.1002/adma.201302223 (2013).
52. Tang, H. J., Yin, H. J., Wang, J. J., Yang, N. L., Wang, D. & Tang, Z. Y. Molecular architecture of cobalt porphyrin multilayers on reduced graphene oxide sheets for high-performance oxygen reduction reaction. *Angew. Chem.* **52**, 5585–9 (2013).

## Acknowledgments

This work was financially supported by National Natural Science Foundation of China (21065005, 21165010), Young Scientist Foundation of Jiangxi Province (20112BCB23006; 20122BCB23011), Science and Technology Support Program of Jiangxi Province (20123BBE50104), Foundation of Jiangxi Educational Committee (GJJ13243 and

GJJ13244), the State Key Laboratory of Electroanalytical Chemistry (SKLEAC201310), and Innovation Foundation for graduate student of Jiangxi Province (YC2012-S052) and Jiangxi Normal University (YJS2012090).

## Author contributions

L.W. and H.H. wrote the main manuscript text. Y.S. and Y.Y. performed the experiments and prepared figures 2–4 and figure 6. Z.L. prepared figure 1. X.L. synthesized the rGO. Z.W. and Y.Y. prepared figure 5 and table 1 and synthesized the PANI-frGO. All authors reviewed the manuscript.

## Additional information

**Competing financial interests:** The authors declare no competing financial interests.

**How to cite this article:** Wang, L. *et al.* Hierarchical Nanocomposites of Polyaniline Nanowire Arrays on Reduced Graphene Oxide Sheets for Supercapacitors. *Sci. Rep.* **3**, 3568; DOI:10.1038/srep03568 (2013).



This work is licensed under a Creative Commons Attribution-NonCommercial-NoDerivs 3.0 Unported license. To view a copy of this license, visit <http://creativecommons.org/licenses/by-nc-nd/3.0>